ELSEVIER

Journal of Fluids and Structures 22 (2006) 109–127

JOURNAL OF FLUIDS AND STRUCTURES

www.elsevier.com/locate/jfs

On fatigue damage accumulation from in-line and cross-flow vortex-induced vibrations on risers

G.S. Baarholm[a,*], C.M. Larsen[b], H. Lie[a]

[a]*MARINTEK, P.O. Box 4125 Valentinlyst, N-7450 Trondheim, Norway*

[b]*Centre for Ships and Ocean Structures (CeSoS), Norwegian University of Science and Technology, N-7491 Trondheim, Norway*

Received 4 September 2004; accepted 18 July 2005

Available online 21 October 2005

Abstract

Large-scale model tests of a tensioned steel riser were performed at Hanøytangen outside Bergen, Norway in 1997. The length of the model was 90 m and the diameter was 3 cm. The information from these tests consists of measured bending strains, tension, flow speed and all relevant riser data. In this work, this information is reexamined in an attempt to improve our understanding of vortex-induced vibrations (VIV) for cases with very high order of responding modes. The aim is in particular to study the relative importance of in-line (IL) and cross-flow (CF) vibrations for fatigue damage accumulation. It is shown that fatigue damage is proportional to U^{2m+1} (U is the flow velocity) when the modes are dominated by tension. When bending controls the modes, the fatigue damage is proportional to U^{m+1}. A linear SN-curve with slope parameter $m = 3$ is used. The Hanøytangen riser fatigue damage goes as U^7 for the lowest velocities and U^4 for the highest current velocities. Based on the Hanøytangen data, it seems that the transition velocity between the tension and the bending-stiffness-dominated regions is at the current velocity that gives response at a mode number where a tensioned string and an untensioned beam have equal eigenfrequencies. IL response has a significant contribution to fatigue for cases dominated by the lowest modes. The reason is that IL oscillations will take place at double the frequency of those in CF. For a tension-controlled case, this corresponds to a mode with half the wavelength, while a bending-controlled case will tend to have a wavelength ratio of $\sqrt{2}$. Since the curvature for a given amplitude increases with the inverse modal wavelength squared, fatigue from IL tends to dominate for cases with tension-controlled modes (low current speed), while CF will dominate for bending-controlled modes (high current speed). This tendency is clearly seen in the experimental data for both CF and IL responses. Fatigue damage is calculated directly from the measured data and compared to results found by using a computer program based on a semi-empirical method. The program is able to calculate response frequencies, response amplitudes and fatigue damage. The method is limited to account for CF vibrations only. Computed results are compared to measurements. The agreement is in general good, but some discrepancy is seen for cases with high current velocity. In these cases, the real response contains high mode orders (above 25) and tends to have a stochastic nature, while the VIV-analysis model assumes that the response takes place at a limited number of discrete frequencies. Further development of the empirical model is therefore needed.

*Corresponding author. Tel.: +47 73 59 55 00; fax: +47 73 59 57 76.

E-mail address: Gro.Sagli.Baarholm@marintek.sintef.no (G.S. Baarholm).

0889-9746/$ - see front matter © 2005 Elsevier Ltd. All rights reserved.

doi:10.1016/j.jfluidstructs.2005.07.013

1. Introduction

Empirical models for VIV prediction of slender marine structures have been applied since the early eighties. Such models have traditionally been based on data from oscillation tests with short (2-D) cylinder sections, and underlying assumptions on how to apply these results to predict the response of a flexible beam in a sheared current. This is not trivial, since the experiments deal with uniform current and one eigenfrequency, while the real case has an unlimited number of vortex-shedding frequencies, eigenfrequencies and mode-shapes. The simplest approach is to assume uniform current and cross-section properties, and presuppose that the response will appear at an eigenfrequency and have the shape of the associated mode-shape, see Larsen and Bech (1986). They applied a simple relationship between response amplitudes found from rigid cylinder tests and modal amplitudes for a flexible pipe, and included both cross-flow (CF) and in-line (IL) vibrations. Today's empirical models are more sophisticated and give a better understanding of the behavior of a flexible beam in a sheared current. The research effort that has made this improvement possible has been substantial. An overview of recent research on the basic VIV phenomenon and empirical models relevant for slender marine structures is found in ISSC (2003), Larsen (2000) and Chaplin et al. (2004).

Today's development takes place along two different lines. Empirical models such as SHEAR7, Vandiver and Lee (2003); VIVANA, Larsen et al. (2001); VIVA, Triantafyllou et al. (1999) and ViCoMo, Moe et al. (2001) are developed to solve engineering problems. They have, however, some common shortcomings. The response is assumed to take place at a limited number of discrete frequencies, and the programs are able to calculate CF vibrations only. The alternative to the empirical methods is the use of computationally fluid dynamics (CFD). Hydrodynamic forces are here computed directly from the Navier–Stokes equation, which means that the load frequency is a part of the solution and that both IL and CF response can be included. This approach is extremely computationally demanding and has not so far been applied for practical problems. However, promising progress is seen. Future analysis programs are therefore expected to be based on such methods.

The main reasons why today's empirical methods do not consider IL vibrations has been the lack of data from tests with combined IL and CF response, and that CF response has been assumed to contribute far more to fatigue than IL. Tognarelli et al. (2004) indicates, however, that fatigue damage from IL vibrations may become significant. The purpose of this work is to shed some further light on the significance of CF versus IL response, and to present measurements from other experiments where both response types have been present. How to use this information in an empirical model will not be discussed, but it is hoped that these results can support such development.

2. The Hanøytangen experiment

Large-scale model tests of a tensioned riser were performed at Hanøytangen, outside Bergen on the west coast of Norway in 1997 (Huse et al., 1998). The test set-up is illustrated in Fig. 1. The test site is a deep water quay. The water

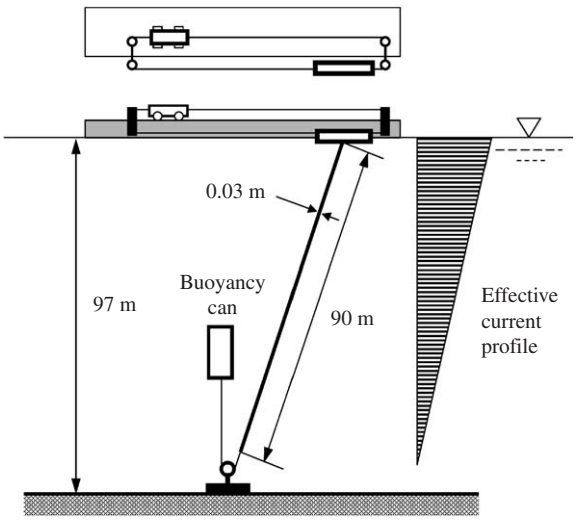

Fig. 1. Test set-up at Hanøytangen.

depth is 97 m. The riser model was attached to a floating vessel that was pulled by a rope system and a vehicle on the quay. The riser model was kept in constant tension by a buoyancy arrangement as seen in Fig. 1. By moving the vehicle at a constant speed, the riser was exposed to a nearly triangular current profile. Tests with one and two risers were carried out. The riser was fitted with transducers for measuring the bending moment in two directions every 3 m down the riser, which means that IL- and CF-induced moments were measured at 29 positions. In addition, 2-D inclinometers and tension transducers were located at both ends. Originally, the objectives of the experiments were to develop testing techniques and provide experimental data on the following:

(i) VIV response of deep sea risers in sheared current;
(ii) effective IL drag amplification of vibration risers;
(iii) criteria for on-set of collision between risers due to wake interaction between individual risers.

The original project included some processing of data recorded from the tests, in particular related to the tandem riser tests and drag amplification. Extended analysis of the data was initiated in 2002. A novel analysis technique was applied for calculation of response amplitudes; see Kaasen and Lie (2005). The present work is based on results obtained in this last study.

3. Analysis procedure for cross-flow VIV

All analyses of vortex-induced vibrations reported in this paper have been carried out using the computer program VIVANA, see Larsen et al. (2000, 2001) and Yttervik et al. (2003). The purpose of VIVANA is to calculate VIV of slender marine structures such as risers, free span pipelines and cables subjected to ocean current. Depending on the length of the structures, cross-section variations and current profile, the riser may experience single- or multi-frequency response. Both response types can be analyzed, but VIVANA is at present limited to compute vibrations orthogonal to the current velocity (CF) only. Hence, IL VIV is not considered.

VIVANA is linked to the RIFLEX program system that has the capability to analyse a large variety of slender marine structures; see Fylling et al. (1995). The analysis method is based on a 3-D finite element formulation that in principle may take any 3-D effects into account. Distribution of tension, mass, bending stiffness, diameter and hydrodynamic coefficients along the riser can be arbitrary. The response is assumed to appear at selected eigenfrequencies, but since added mass depends on the frequency and local flow velocity, these response frequencies will be different from eigenfrequencies valid for still water. Key features of the analysis model will be given in the following. Further details are given by Larsen et al. (2000).

3.1. Hydrodynamic coefficients

The analysis model is based on empirical coefficients for lift force, added mass and damping. All coefficients will depend on the nondimensional frequency,

$$\hat{f} = \frac{f_{\text{osc}} D}{U}, \tag{1}$$

where f_{osc} is the oscillation frequency, D is the diameter and U is the flow velocity. Both D and U may vary along the riser, which means that all coefficients also may vary.

The lift coefficient C_L will depend on the oscillation amplitude A as well as on the frequency. This is obtained by use of a lift coefficient curve as shown on Fig. 2. C_L is here given as function of the nondimensional amplitude A/D, and the curve is defined by four parameters as illustrated in the figure. These parameters are given as functions of the nondimensional frequency. Hence, if the response frequency is known, the C_L versus A/D curve will be known at any location along the riser.

The added mass coefficient is assumed to be independent of the amplitude and is therefore given as a simple function of the frequency only.

The damping model proposed by Venugopal (1996) is used in VIVANA. It is partly based on Gopalkrishnan's (1993) experiments on an oscillating cylinder. Vikestad (1998) made other experiments and confirmed that the damping model is conservative, meaning that real damping is normally higher than that predicted by the model. This model applies different formulations for damping in high and low flow velocity regions. The VIVANA model has in addition included a damping term for high response amplitude in order to take the self-limiting character of VIV into account. This term

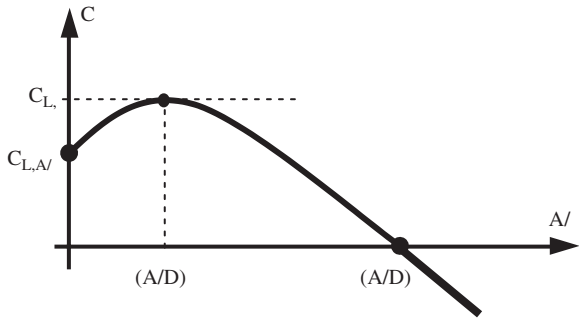

Fig. 2. Lift coefficient curve as defined in VIVANA.

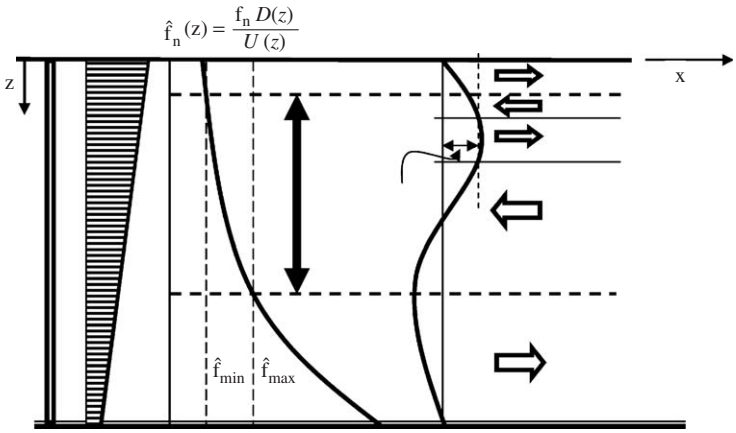

Fig. 3. Energy balance for vibrating riser in sheared current.

follows directly from the lift coefficient curve in Fig. 2. If the amplitude exceeds $(A/D)_{C_L=0}$, the lift coefficient is seen to become negative. This means that the lift force will have a phase shift of 180° and the force will act against the velocity. Hence, the lift force will dissipate energy and thereby contribute to damping. This effect is particularly important for cases with uniform flow velocity. Fig. 3 illustrates the energy balance for a case with all the mentioned damping types.

3.2. Identification of response frequencies

Before a dynamic analysis can be carried out, it is necessary to find the static equilibrium condition. The next step will be to identify possible response frequencies for VIV. A response frequency is assumed to be a single eigenfrequency, but since added mass will vary with frequency and flow velocity, iterations are required. Such iterations must be carried out for a large number of eigenfrequencies.

A subset of response frequency candidates will define the complete set of possibly active frequencies. These are found from an excitation range criterion defined in terms of an interval for the nondimensional frequency where excitation can take place. The present study applies to an interval of

$$0.125 < \hat{f} < 0.2, \tag{2}$$

By use of this interval, one can find an excitation zone for each response frequency, and eigenfrequencies without an excitation zone cannot become active. Identification of the excitation zone is illustrated in Fig. 3.

The next step is to find the dominant eigenfrequency. A criterion based on an integral over the excitation zone L_E for each response frequency has been applied in the theoretical VIV model. The criterion is expressed as

$$\int_{L_E} U^2(z) D^3(z) \left(A/D\right)_{C_L=0} \mathrm{d}z, \tag{3}$$

where $(A/D)_{C_L=0}$ is found from the lift coefficient curve, see Fig. 2. The frequency candidates are ranked according to the numerical value of this integral. The dominant frequency will be dedicated to its complete excitation zone in the succeeding response analysis. The division of excitation zones between the other response frequencies will be discussed later.

3.3. The response analysis

The frequency response method is used to calculate the dynamic response at the dominant frequency identified in the previous step. The lift and damping coefficients depend on the local response amplitude. Hence, the response must be found by an iteration procedure. A part of this iteration is to have the correct phase between lift force and response at all positions along the pipe. The result is the complete description of exciting forces and damping coefficients along the pipe.

The frequency response method is well suited for this application since the loads are assumed to be acting at a known discrete frequency. Use of the finite element method will give the dynamic equilibrium equation as

$$\mathbf{M}\ddot{\mathbf{r}}(t) + \mathbf{C}\dot{\mathbf{r}}(t) + \mathbf{K}\mathbf{r}(t) = \mathbf{R}(t), \tag{4}$$

where $\mathbf{M}$ is the mass matrix, $\mathbf{C}$ is the damping matrix and $\mathbf{K}$ is the stiffness matrix. $\mathbf{r}, \dot{\mathbf{r}}$ and $\ddot{\mathbf{r}}$ are the displacement, velocity and acceleration vectors, respectively. The external loads will in this case be harmonic, but loads at all degrees of freedom are not necessarily in phase. It is convenient to describe this type of load pattern by a complex load vector $\mathbf{X}$ with harmonic time variation at a known frequency ω,

$$\mathbf{R}(t) = \mathbf{X}e^{i\omega t}. \tag{5}$$

The response vector will also be given by a complex vector and a harmonic time variation,

$$\mathbf{r}(t) = \mathbf{x}e^{i\omega t}. \tag{6}$$

Eqs. (5) and (6) can now be introduced into Eq. (4). The mass and damping matrices can be split into structural and hydrodynamic parts. Hence, we have

$$-\omega^2(\mathbf{M}_S + \mathbf{M}_H)\mathbf{x} + i\omega(\mathbf{C}_S + \mathbf{C}_H)\mathbf{x} + \mathbf{K}\mathbf{x} = \mathbf{X} \tag{7}$$

The damping matrix $\mathbf{C}_S$ represents structural damping and will normally be assumed to be proportional to the stiffness matrix. $\mathbf{C}_H$ contains terms from hydrodynamic damping.

The response vector $\mathbf{x}$ is complex. The vector describes a harmonic response at all nodes, but the responses may have different phase. This means that the response will not necessarily appear as a standing wave, but may have contributions from travelling waves. From a mathematical point of view, $\mathbf{x}$ is equivalent to a complex mode found from the damped eigenvalue problem.

Since the load vextor $\mathbf{X}$ depends on the response vector $\mathbf{x}$, Eq. (7) must be solved by iteration. The aim of this iteration is to identify a load vector that gives a consistent response vector in the sense that both amplitudes and phases are correct at all positions, and also in accordance with the local flow conditions.

In the general case, the dominant frequency will not have an excitation zone that covers the total riser length. Consequently excitation may take place at other frequencies in zones outside the primary zone. A similar analysis must therefore be carried out for other frequencies, but the excitation zones for these frequencies will be reduced according to the zones already taken by the more dominant ones. Hence, zone overlaps are avoided, and the dominant frequency will have the largest possible zone.

When the VIV response analysis is completed, we are left with N complex response vectors $\mathbf{x}_1, \mathbf{x}_2, \ldots, \mathbf{x}_N$. These are used in combination with the element stiffness matrices and cross-section properties to derive the time series of stresses. Hence, a multifrequency response at discrete time increments is obtained. Stress cycles are counted by the Rainflow counting method (Anzai and Endo, 1979), and the fatigue damage is found by Miner summation of stress cycles (Miner, 1945).

4. Fatigue Damage

Applying beam theory, the normal stress in the longitudinal direction of the riser as a result of global bending and axial force variation is given as

$$\sigma_z(x, y) = \frac{F_z}{A_z} + \frac{y}{I_{xx}}M_x + \frac{x}{I_{yy}}M_y. \tag{8}$$

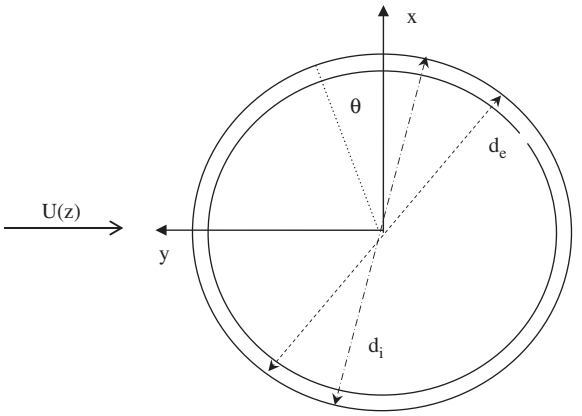

Fig. 4. Illustration of axis orientation and current direction for a cross-section.

The axial force in the longitudinal direction is denoted as F_z, while M_x and M_y are the bending moments about the x- and y-axes. The cross-sectional area is denoted as A_z and the moments of inertia about the x- and y-axes are denoted as I_{yy} and I_{xx}, respectively. For a circular cross-section, the x and y values on the circumference are functions of the external diameter of the riser and the angle θ, see Fig. 4. Relating M_y to bending caused by CF VIV and M_x to VIV, the stress at $\theta = 0^\circ$ is due to CF VIV. The stress at $\theta = 90^\circ$ is caused by IL VIV. The two moment components will respond at different frequencies. If the axial force variation is assumed to be negligible, the stress is given as a function of time and angle by

$$\sigma_z(\theta, t) = \frac{1}{2I_{xx}} d_{de} \sin\theta M_x(t) + \frac{1}{2I_{yy}} d_e \cos\theta M_y(t), \tag{9}$$

where d_e is the external diameter, see Fig. 4.

Applying the Miner summation, the fatigue damage is given by

$$D = \sum_{i=1}^{N_{\text{bin}}} \frac{n_i}{N_i}, \tag{10}$$

where N_i is the number of cycles to failure and n_i is the number of stress cycles at stress range $\Delta\sigma_i$ and N_{bin} is the number of stress range bins used in the Rainflow procedure. The SN-curve is defined as

$$\log N_i = \log a - m \log \Delta\sigma_i, \tag{11}$$

where a is the scale parameter and m is the slope parameter. Hence, the fatigue damage can be written as

$$D = \frac{1}{a} \sum_{i=1}^{N_{\text{bin}}} n_i (\Delta\sigma_i)^m. \tag{12}$$

An alternative method for calculating the fatigue damage is to assume that the stress ranges are narrow-banded and Rayleigh-distributed. For a linear SN-curve with no fatigue limit, the fatigue damage can be found from [see Det Norske Veritas (1988)]

$$D = \frac{f_0 T_0}{a} \left[\left(2\sqrt{2m_0} \right)^m \Gamma\left(1 + \frac{m}{2}\right) \right], \tag{13}$$

where T_0 is the time in seconds, f_0 is the zero-up-crossing frequency and m_0 is the zeroth spectral moment of the stress process, m and a are the SN-curve parameters, while $\Gamma(\,)$ is the complete gamma function.

5. Preliminary analysis of a tensioned riser

Some key features of riser dynamics and associated fatigue damage can be illustrated by inspecting the eigenfrequencies and mode-shapes of a tensioned beam with moment free supports at both ends. The eigenfrequencies

for a tensioned string and an untensioned beam with equal length L and mass per unit length m are given by

$$f_{n,\text{ string}} = n\frac{1}{2}\sqrt{\frac{T}{mL^2}}, \tag{14}$$

$$f_{n,\text{ beam}} = n^2\frac{\pi}{2}\sqrt{\frac{EI}{mL^4}}, \tag{15}$$

where n is the mode number, T is the constant tension in the string and I is the moment of inertia of the beam. The actual riser will not have constant tension along its length. However, Eq. (14) represents a good approximation if the tension variation is moderate and T is set equal to the spatially averaged tension.

The tensioned string and untensioned beam will have identical mode-shapes if the ends have moment-free supports. The mode-shape for eigenfrequency n is given by

$$\Phi_n(z) = A_0 \sin\left(\frac{n\pi}{L}z\right), \tag{16}$$

where A_0 is an undetermined amplitude. This mode-shape will give identical modal mass for all modes, and also for the string and beam case. The nth eigenfrequency for the tensioned beam, f_{n,t_beam} can therefore be found from

$$f_{n,t\_\text{beam}} = \sqrt{f_{n,\text{string}}^2 + f_{n,\text{beam}}^2}. \tag{17}$$

The eigenfrequency as a function of the mode number n for the Hanøytangen riser model is shown in Fig. 5. Values for an untensioned beam, tensioned string and tensioned beam are shown. The eigenfrequency for the tensioned riser is seen to follow the tensioned string case for the lower modes, and then become closer to the untensioned beam case as the mode number increases. This means that the stiffness of the riser will be tension-dominated for the lower modes. The bending stiffness becomes increasingly important for the increasing mode order.

If the riser responds at one single frequency f_n and the response shape consists of the associated mode-shape Φ_n only, the maximum bending stress is given as

$$\begin{aligned}\sigma_{\max}(z,t) &= E\varepsilon(z,t) = E\frac{r_e}{R(z,t)} = Er_e\frac{\partial^2}{\partial z^2}x(z,t)\\ &= -Er_e x_0\left(\frac{n\pi}{L}\right)^2 \sin\left(\frac{n\pi z}{L}\right)\sin(\omega t),\end{aligned} \tag{18}$$

where E is the modulus of elasticity, ε is the strain, r_e is the external radius of the pipe, R is the radius of curvature of the pipe and x_0 is the displacement amplitude for the modeshape. As can be seen from Eq. (18), the bending stress is proportional to n^2, where n is the active mode number.

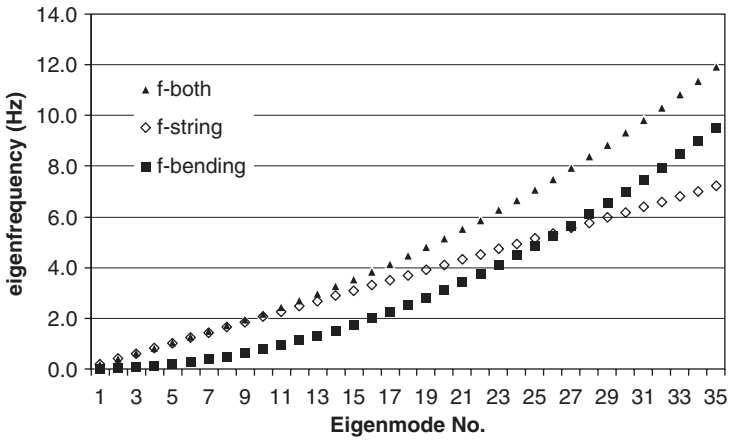

Fig. 5. Estimates of natural frequencies for the Hanøytangen riser based on analytical solution of a string in tension and a beam (f-string = eigenfrequencies for a tension string, f-bending = eigenfrequencies for a beam, f-both = eigenfrequencies for a beam in tension).

The fatigue damage can be related directly to the current velocity. The response frequency will, in general, be close to the vortex shedding frequency. Accordingly, we may assume that the response frequency f_n can be written as

$$f_n = \frac{\mathrm{St}U}{2r_e}, \tag{19}$$

where St is the Strouhal number which is almost constant and close to 0.2 for subcritical values of the Reynolds number. Combining this Eq. (19) with Eqs. (12) and (13), the mode numbers for a tensioned string and an untensioned beam are given as

$$\begin{aligned} &\text{Tensioned string}: \quad n = \frac{\mathrm{St}U}{r_e}\sqrt{\frac{mL^2}{T}} \quad \text{or} \quad n \propto U, \\ &\text{Untensioned beam}: \quad n = \frac{\mathrm{St}U}{\pi r_e}\sqrt{\frac{mL^4}{EI}} \quad \text{or} \quad n^2 \propto U. \end{aligned} \tag{20}$$

It is seen that the eigenfrequency order n is proportional to U for a tensioned string. For the untensioned beam the case n^2 is proportional to U.

Since VIV amplitudes are self-limiting, one can assume that the response amplitude x_0 in Eq. (18) is independent of the current velocity. According to Eqs. (12) and (13), one may see that the following proportionality relationship applies,

$$D \propto f_n \sigma^m. \tag{21}$$

By combining Eqs. (16)–(19), one can write

$$\begin{aligned} &\text{Tensioned string}: \quad D \propto f_n \sigma^m \propto U(n^2)^m \propto U(U^2)^m \propto U^{2m+1}, \\ &\text{Untensioned beam}: \quad D \propto f_n \sigma^m \propto U(n^2)^m \propto U(U)^m \propto U^{m+1}. \end{aligned} \tag{22}$$

For a linear SN curve, the slope parameter m is often seen to be 3.0 (Norsok, 1998). Looking at Fig. 5, we see that low current velocity will tend to activate tension-dominated modes. Bending-dominated modes will appear for the higher velocities. This means that the fatigue damage of a riser such as the Hanøytangen riser will have a U^7 trend at low velocities. A U^4 trend will gradually take over for higher velocities.

If current and response measurements are available, the transition point between the two regions can be found by studying the calculated fatigue damage as a function of the current speed.

It is also possible to study the relative influence from IL and CF vibrations by using the equations above. The ratio between IL and CF stresses can be found from Eq. (18),

$$\frac{\sigma_{\mathrm{IL}}}{\sigma_{\mathrm{CF}}} = \frac{x_{0,\mathrm{IL}}}{x_{0,\mathrm{CF}}}\frac{n_{\mathrm{IL}}^2}{n_{\mathrm{CF}}^2}. \tag{23}$$

Combining Eqs. (13) and (23) gives

$$\frac{D_{\mathrm{IL}}}{D_{\mathrm{CF}}} = \frac{f_{\mathrm{IL}}}{f_{\mathrm{CF}}}\left(\frac{\sigma_{\mathrm{IL}}}{\sigma_{\mathrm{CF}}}\right)^m = \frac{f_{\mathrm{IL}}}{f_{\mathrm{CF}}}\left(\frac{x_{0,\mathrm{IL}}}{X_{0,\mathrm{CF}}}\frac{n_{\mathrm{IL}}^2}{n_{\mathrm{CF}}^2}\right)^m, \tag{24}$$

where f_{IL} is known to be $2f_{\mathrm{CF}}$ for 2-D tests. This is not necessarily true for flexible beams. However, experience from the Hanøytangen experiment confirms that this relationship is valid. Fig. 6 shows auto spectra for measured IL and CF bending moments at the same cross-section of the riser. The spectra exhibit multiple frequencies for both CF and IL. The peaks and bandwidth of the IL response appear at the double frequency as CF. This simple relationship between the two frequencies will be applied in this study. Combining the factor 2 with the eigenvalue from Eqs. (14) and (15), one sees that the ratio between active IL and CF modes $n_{\mathrm{IL}}/n_{\mathrm{CF}}$, will be different for the tensioned string and untensioned beam case,

$$\begin{aligned} &\text{Tensioned string}: \quad n_{\mathrm{IL}} = 2n_{\mathrm{CF}}, \\ &\text{Untensioned beam}: \quad n_{\mathrm{IL}} = \sqrt{2n_{\mathrm{CF}}}. \end{aligned} \tag{25}$$

These relationships are asymptotic values for increasing length of strings and beams, but will be used here for the sake of simplicity.

The ratio between IL and CF amplitudes has been investigated by Baarholm et al. (2004). From the Hanøytangen experiments and other published data, they found that this ratio varied with the mode order. For low modes the ratio

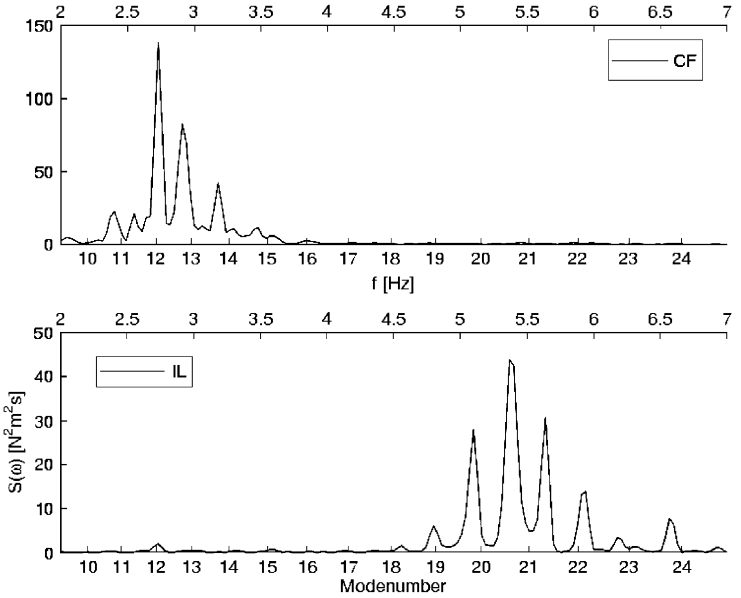

Fig. 6. Example of spectra for measured CF- and IL-induced bending moments at the same cross-section (CF = cross-flow, IL = in-line).

Table 1
Key data for the riser experiments

Outer diameter	(m)	0.030
Length	(m)	90
Inner diameter	(m)	0.026
Modulus of elasticity	(N/m^2)	2.1×10^{11}
Riser density	(kg/m^3)	3211
Mass	(kg/m)	2.27

was found to be approximately 0.5, while 0.3 was seen for higher modes. Assuming that low modes are tension controlled and high modes are controlled by bending stiffness, one can apply Eq. (22) to obtain an estimate for relative fatigue damage. A linear SN curve with slope parameter $m = 3$ is used. The results are:

$$\begin{aligned} &\text{Tensioned string, low modes :} \quad \frac{D_{\mathrm{IL}}}{D_{\mathrm{CF}}} = 16, \\ &\text{Untensioned beam high modes :} \quad \frac{D_{\mathrm{IL}}}{D_{\mathrm{CF}}} = 0.43. \end{aligned} \tag{26}$$

These results are, of course, rough estimates; but one may still expect IL vibrations to be more important than CF ones for cases with tensioned-controlled modes. CF will tend to become more important for bending-stiffness-controlled cases. The relative influence between the two vibration types will be case dependent. The current velocity with equal influence will therefore have a considerable variation from case to case. This point will be further addressed in the following case study.

6. Case study

The Hanøytangen riser model is exposed to a sheared current profile. The current speed ranges from $U_{\max}$ at the free surface to almost zero current at the lower riser end, see Fig. 1. Key data for the riser model are given in Table 1.

Throughout the fatigue analysis, the D curve from the NORSOK standard (1998) is applied. The curve chosen is valid for specimens in sea-water exposed to free corrosion. This is a linear SN-curve in a log–log scale with the slope

Table 2
SN-curve parameters

SN-curve	$\log K$	m	Ref. thickness (mm)
D	11.687	3.0	25

parameter m equal to 3. Hence, applying other similar curves with $m = 3$ will just introduce a scale difference in the estimated fatigue damage.

The SN-curve parameters applied are listed in Table 2. The stress concentration factor is set to 1.0 for all cases.

7. Results and discussion

7.1. Fatigue damage based on experimental data

Twenty-one test cases with available IL and CF measurements have been investigated. The maximum current velocity, $U_{\max}$, in the sheared current profile ranges from 0.16 to 1.96 m/s. High quality measurements were produced at 23 out of 29 instrumented positions. The fatigue stress is calculated along the riser on the basis of bending strain measurements in two orthogonal planes. At each section, the damage is calculated at ten points from 0° to 180° positioned on the outer circumference of the cross-sectional area in order to find the maximum fatigue damage.

The fatigue damage is calculated using Miner summation assuming Rayleigh distributed stress ranges according to Eq. (13). This is denoted as *Closed-form* in the following discussion. In addition, the stress cycles are counted using using the Rainflow counting method.

The maximum fatigue damage in a cross-section i is taken to be

$$D^i_{\max} = \max_{\text{all } \theta} D(\theta), \tag{27}$$

where $D(\theta)$ is the fatigue damage at angle θ on the cross section, as in Fig. 4. The maximum fatigue damage is referred to as max in the plots. Similarly, the maximum fatigue along the riser in a given test case is taken to be

$$D_{\max} = \max_{i=1,23} D^i_{\max}. \tag{28}$$

The resulting fatigue damage along the riser, $D^i_{\max}$, for $U_{\max} = 0.64\,m/s$ is shown in Fig. 7. The upper figure shows the maximum fatigue damage as well as fatigue damage due to CF and IL VIV. The damage is calculated using Rainflow counting. The two figures at the bottom compare CF and IL fatigue damage for CF and IL using both the Rainflow method and the closed-form equation. As can be seen, the analytical method leads to slightly larger fatigue damage than Rainflow counting at all points along the riser. For practical purposes, this difference is considered negligible. The results imply that the stress ranges are narrow-banded and close to a Rayleigh distribution.

The fatigue data for all current profiles and positions along the riser is given in Figs. 8–12. Fig. 8 shows the maximum fatigue damage along the riser, $D_{\max}$, as a function of the maximum current speed. The continuous line shows the maximum fatigue damage. The open squares and filled circles represent the contribution from CF and IL fatigue damage, respectively. It is interesting to see that the line for maximum damage follows IL or CF values for almost all cases, at least when presenting the data in logarithmic scale. This means that one of the two contributors normally will dominate fatigue accumulation.

It is important to note that the IL response will tend to give higher bending stresses for cases with tension-controlled modes than for bending-stiffness-controlled cases. The reason is explained in Section 5. The IL response frequency will be twice the CF frequency. For the tension-controlled case, this will correspond to an IL mode with half the wavelength as for the CF mode, while the wavelength ratio will become $\sqrt{1/2}$ for the bending-stiffness-controlled case. Since the response amplitude is almost independent of the mode number, IL stresses will be higher for the shorter mode. The results from measurements clearly demonstrate that this effect is present, since IL fatigue tends to dominate for the low current case with tension-controlled modes, while CF fatigue is more important for high current speeds with bending-stiffness-controlled modes.

Based on the information in Section5, the fatigue damage as a function of the flow velocity may be split the in two regions in a current velocity plot. Applying the SN-curve given in Table 2, the fatigue damage in the region below the transition velocity is proportional to U^7 (tension- dominated modes), and proportional to U^4 (bending-dominated

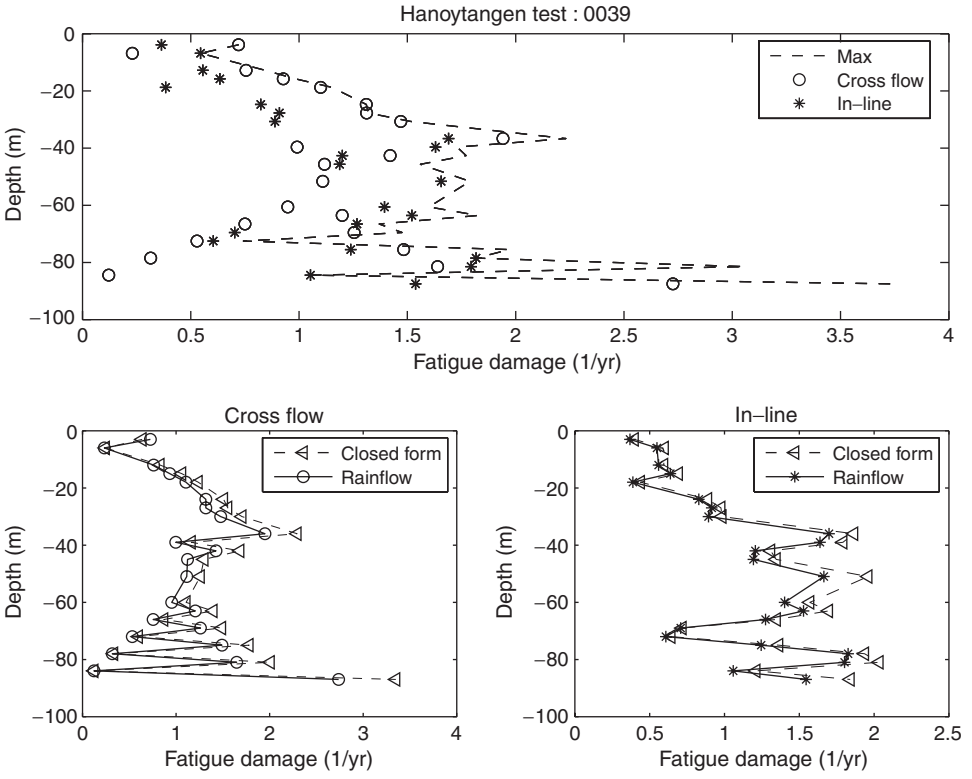

Fig. 7. Fatigue damage calculated using the measured bending moments along the riser, $U_{\max} = 0.64\,\mathrm{m/s}$.

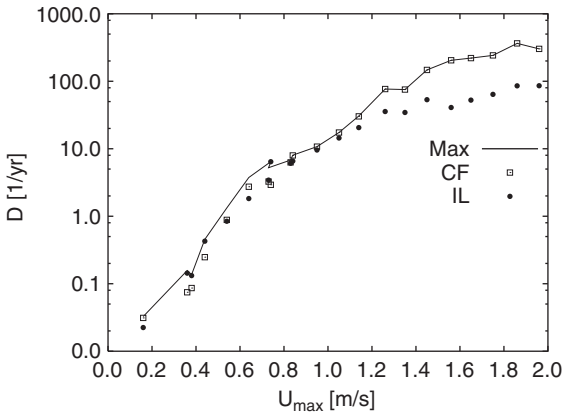

Fig. 8. Maximum fatigue damage as a function of maximum current velocity.

modes) in the region above. The IL vibrations have approximately twice the frequency and twice the mode number as CF vibrations. The IL fatigue damage rate should therefore have a transition velocity at approximately half the current velocity as for CF. Looking at Fig. 8, it seems that CF has a transition point at approximately 1.3 m/s and IL at 0.7 m/s. Hence, two sets of curves are fitted to the IL and CF fatigue data. The curves are given as

$$D = \begin{cases} \beta_1 U^7, & U < U_{\text{transition}}, \\ \beta_2 U^4, & U \geqslant U_{\text{transition}}. \end{cases} \tag{29}$$

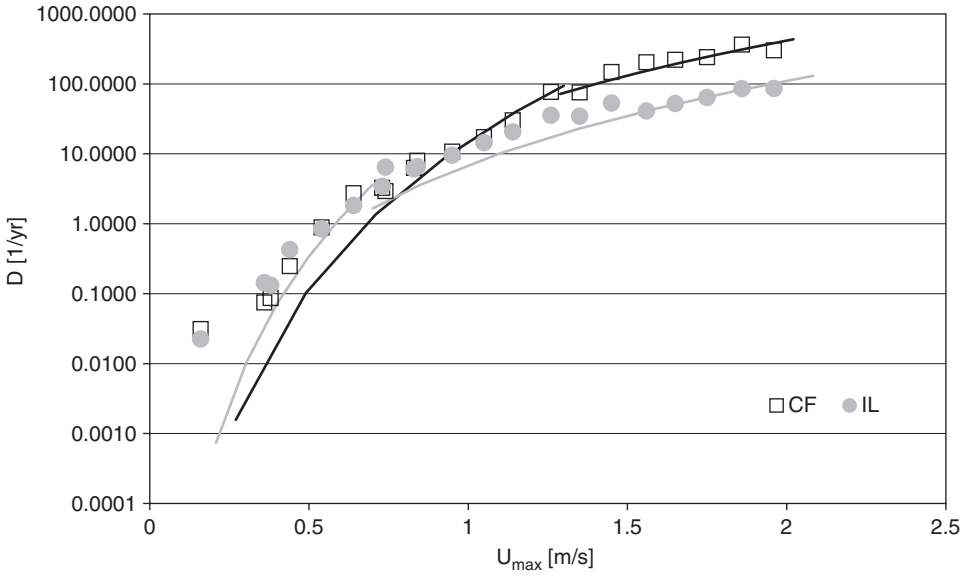

Fig. 9. Curve fit for IL and CF maximum fatigue damage.

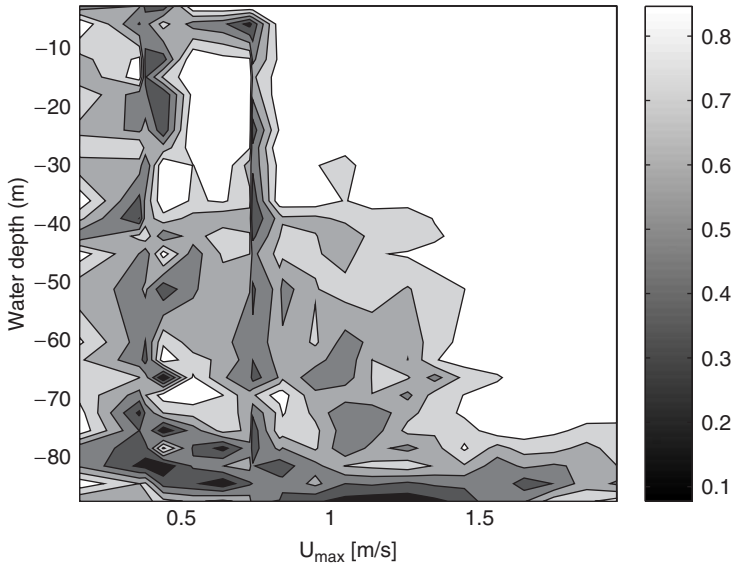

Fig. 10. The ratio between damage from CF and maximum damage as function of maximum current velocity and water depth.

The resulting curve fits for IL (grey circles and line) and CF (black squares and line) fatigue damage are shown in Fig. 9. The scale parameter, β, is listed in Table 3. Looking at Figs. 10–12, one notices that the transition velocities divide the fatigue data into three regions. The area below 0.7 m/s is dominated by IL fatigue and modes are tension-controlled. There is an intermediate region between the two transition velocities where IL and CF are equally important. For the region above 1.3 m/s, CF fatigue has the major contribution and bending stiffness is controlling the active modes.

It is interesting to observe the ratio between eigenfrequencies at the transition velocities. The transition velocity for IL response is 0.7 m/s. According to Fig. 14, the response will be dominated by mode 15. From Fig. 5 it can be seen that the

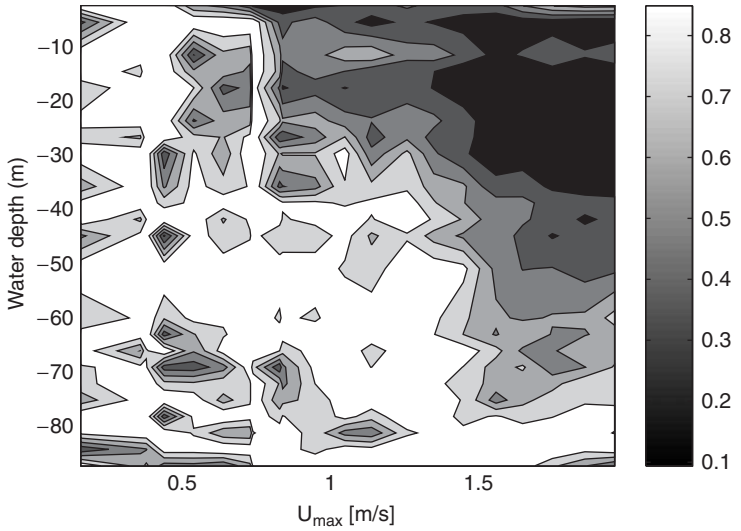

Fig. 11. The ratio between damage from IL and maximum damage as function of maximum current velocity and water depth.

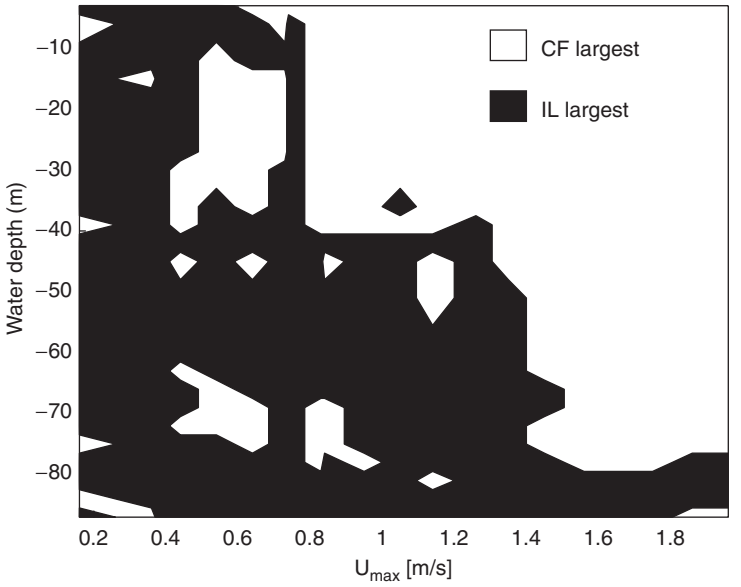

Fig. 12. Illustration of CF and IL dominance as a function of maximum current velocity and water depth (0 m = top of the riser, −90 m = bottom of riser).

associated eigenfrequency for the tensioned beam is approximately 3.5 Hz. The IL response will, however, appear at the double frequency, i.e. 7.0 Hz. This corresponds to mode 26. From Fig. 5, it is seen that this is the mode where the tensioned string and the untensioned beam have equal eigenfrequencies, both approximately equal to 5.6 Hz.

The CF transition velocity is found to be 1.3 m/s. According to Fig. 14, the 25th mode will dominate. For this mode number the tensioned string and untensioned beam eigenfrequencies are close, see Fig. 5. Hence, the two transition velocities seem to be controlled by the intersection point for string and beam eigenfrequencies. Knowing this, one may easily estimate the transition velocities for a given riser from an eigenvalue analysis and the Strouhal relationship, see Eq. (19).

The fatigue damage for the lowest current velocity in Fig. 9 requires a comment. The damage is seen to be more than one decade higher than predicted by the U^7 curve. The most probable reason for this is background current at the test

Table 3
Scale parameter, β

Exponent	CF	IL
4	15.04	43.90
7	26.03	6.93

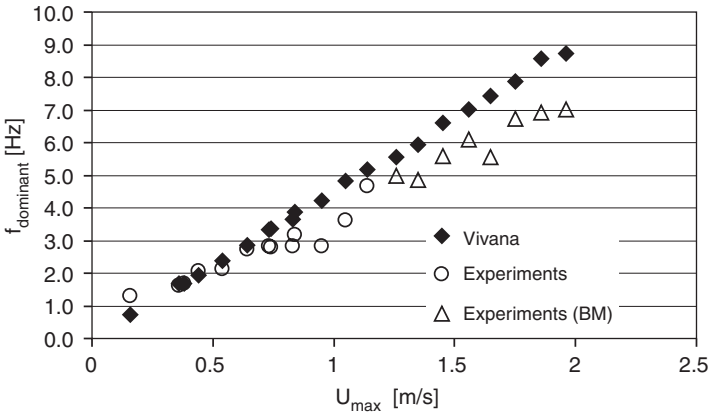

Fig. 13. Comparison between measured and calculated dominant frequency (VIVANA: dominant frequency calculated using the theoretical VIV model; Experiments: measured dominant frequency; Experiments (BM): dominant frequency based on spectra of measured bending moments).

site for this specific test case. Maximum and average velocities are 0.16 and 0.08 m/s, respectively, which means that a background current of 0.03–0.06 m/s will increase fatigue damage by a factor of 10. One should therefore be careful to include this particular data point when discussing the trend for fatigue damage versus current velocity.

Fig. 10 shows the ratio between fatigue damage due to CF vibrations, D_{CF}, and maximum fatigue, $D^i_{\max}$, as a function of maximum current velocity and vertical position. Fig. 11 shows the corresponding results for IL vibrations. Fig. 12 indicates the combination of vertical position and current velocity giving the largest IL or CF fatigue damage.

As can be seen in Figs. 10–12, IL vibrations are the major contributior to fatigue damage for the cases with low $U_{\max}$ (0.16–0.74 m/s). Gradually as the flow speed increases (approximately 0.83–1.26 m/s), the CF fatigue damage begins to dominate, but primarily over the top portion of the riser where the flow speed is higher. In the midflow speed cases, the top half or so of the riser is dominated by CF while the bottom is IL dominated. The damage rate is also about the same at the top and bottom of the riser, but the fatigue rate at the top is due to CF VIV and the bottom fatigue rate is caused by IL VIV. For the high current speed cases, the CF fatigue dominates along the total riser length (approximately 1.35–1.96 m/s). The increased influence from CF vibrations for increasing flow velocity is in accordance with the findings in Section 5.

The results may be influenced by the band-pass filter frequencies. The raw data was sampled at a frequency of 100 Hz after analog filtering at 40 Hz [see Huse, (1998)]. Extra noise was detected in some of the channels and was removed by setting band-pass filters for CF and IL vibrations individually. This introduces approximately 10% reduction of the standard deviation of the bending moment. This is discussed in more detail by Lie and Kaasen (2005), who found that this effect might give a 30% reduction of the fatigue damage.

7.2. Comparisons of experimental data and simulated VIV results

The calculated and observed dominant CF frequencies are presented in Fig. 13. All calculations have been carried out using VIVANA, which was described in Section 3. The dominant frequencies found by analysis of the Hanøytangen data [see Lie and Kaasen (2005)], are represented by the circles. VIVANA is seen to give a consistent overprediction of the response frequency. The most probable reason for this is that a fixed Strouhal number of 0.2 was used for all

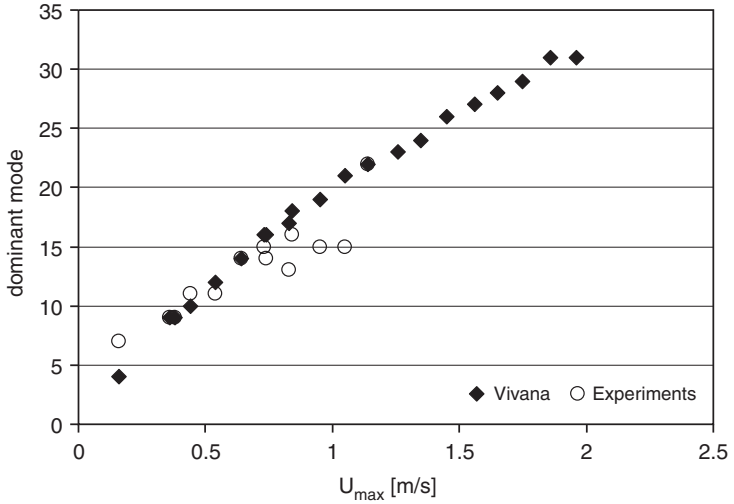

Fig. 14. Comparison between measured and calculated dominating modes (VIVANA: dominant mode calculated using the theoretical VIV model; Experiments: measured dominant modes).

calculations, which might be slightly higher than the correct value. No attempt on tuning the Strouhal number to get a better match was made. There is, however, one important difference between the measured and computed response frequencies that is not seen from Fig. 13. VIVANA will identify some discrete response frequencies, while the true response will have a more stochastic nature, see Fig. 6. This difference is important and calls for further work on methods for analysis of VIV, in particular for cases with a high order of responding eigenfrequencies.

The corresponding dominating mode numbers for CF VIV versus the maximum current speed are shown in Fig. 14. Dominant frequencies and modes are not available for current velocities above $U_{\max} = 1.14\,\mathrm{m/s}$. This is a consequence of the limited number of bending moment transducers, which made a reasonably accurate modal analysis impossible for high-speed cases [see Lie and Kaasen (2005)]. The frequencies in Fig. 13 indicated by triangles are therefore taken from bending moment spectra (Huse et al., 1998, 1999).

The agreement between predictions and observations is in general good, but a systematic overprediction is seen for high velocity cases. The case with lowest current velocity is underpredicted by VIVANA. As previously mentioned, the deviation from the general trend indicates that some background current might have caused too high a response in the test. This conclusion is supported by the difference between calculated and measured response seen here.

Measured and computed fatigue damage as functions of current velocity are presented in terms of contour curves on Figs. 15 and 16. The two plots show similar trends: fatigue will increase for increasing velocity and decrease for increasing depth. The first effect is trivial and follows for increasing frequency and mode order, while the latter is a consequence of local flow speed and damping along the riser.

The calculated fatigue damage is seen to have a significant reduction toward the top of the riser. The explanation for this is that the added mass according to the theoretical VIV model will become low and even negative at this part of the riser because of the high flow velocity. If the mass is low, the wavelength of the mode will become longer. Since curvature decreases with the inverse wavelength square and the fatigue damage is proportional to stress to the third power, the fatigue is highly dependent on the local added mass. The measured response does not have the same strong trend, which may indicate that the idealized added mass model in the theoretical VIV model does not correctly represent the physical situation. However, the discrepancy may also be caused by simplifications in the theoretical excitation model.

Fig. 17 presents the ratio between calculated and measured fatigue damage from CF vibrations as function of velocity and position along the riser. The calculations are seen to overpredict damage for almost all positions on this map, which is not surprising since some conservative assumptions are applied in the theoretical VIV model. The overprediction tends to be larger for increasing velocity. The average value for the ratio is seen to increase from 2 at 0.5 m/s to 6 at 1.8 m/s. The largest discrepancy is seen at the lower end of the riser, where predictions are overestimated by a factor of up to 18. From Figs. 15 and 16, it is seen that the contours from experiments and computations have different trends at the lower end of the riser. The reason for this might be the damping model which is based on experimental data and is tuned to give lower damping than most known results. All cases here have excitation at the upper part of the riser where

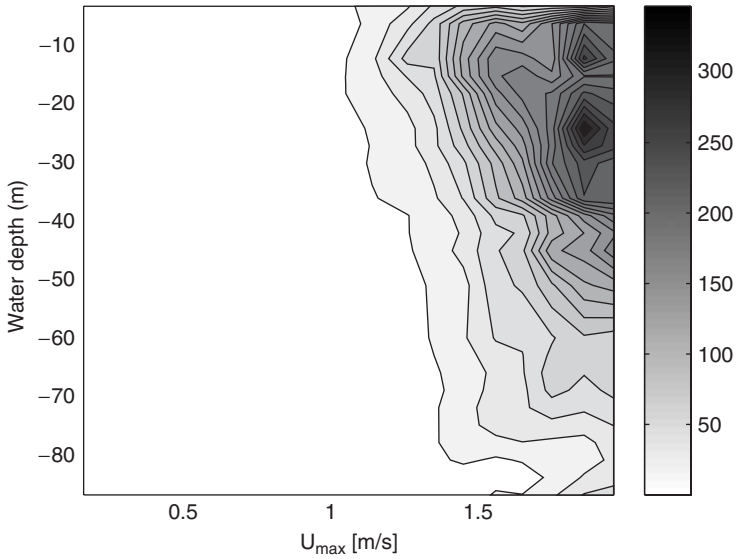

Fig. 15. Measured fatigue [Damage/year] from CF as function of the maximum current velocity and water depth (0 m = top of the riser, −90 m = bottom of riser).

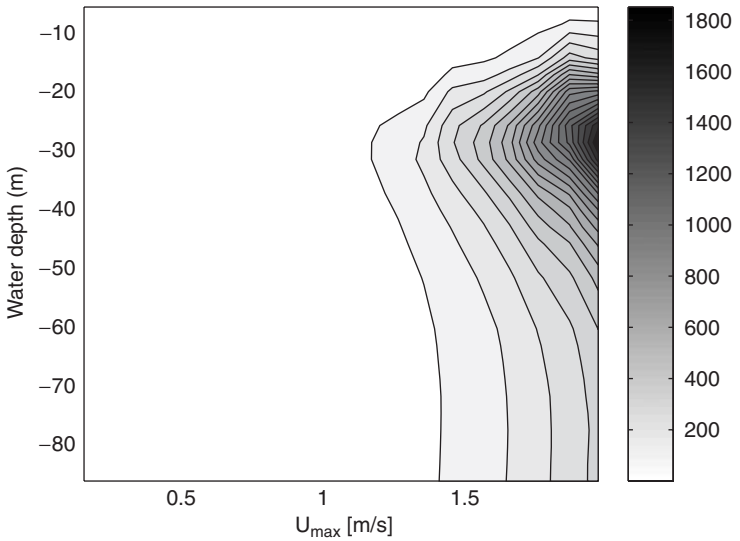

Fig. 16. Calculated fatigue [Damage/year] from CF as a function of the maximum current velocity and water depth (0 m = top of the riser, −90 m = bottom of riser).

the flow velocity is highest, and damping will lead to spatial attenuation downward along the riser. If damping is systematically underpredicted, one will see lower response at the bottom end in the experiments than predicted by the theoretical VIV model. The reason may also be due to differences in the theoretical and real boundary conditions at the end. One should also observe that the largest difference occurs where the fatigue damage is low, which means that it is not crucial for maximum fatigue prediction of the present riser system.

Fig. 18 presents the maximum IL and CF fatigue damage from experiments together with CF predictions. The fatigue damage is calculated satisfactorily compared to experimental results for velocities up to 1.3 m/s corresponding to dominant mode orders up to 22. When the current speed increases, the fatigue increases and the fatigue damage is

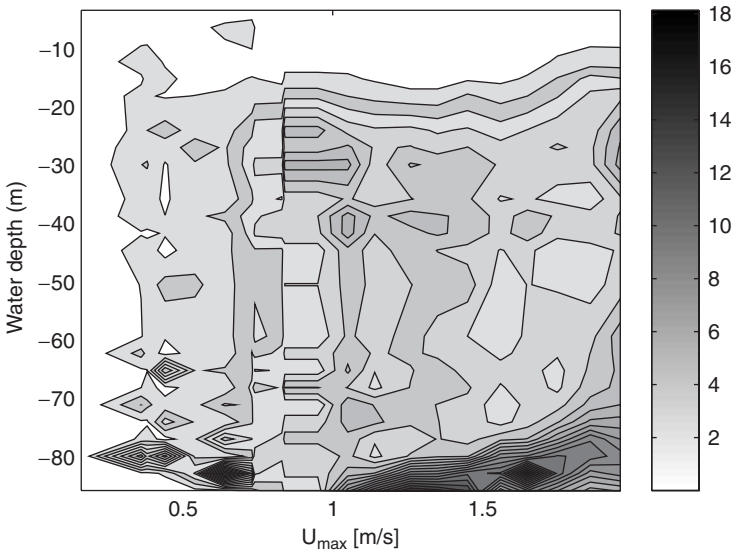

Fig. 17. Ratio between calculated and measured CF fatigue damage as function of maximum current velocity and water depth (0 m = top of the riser, −90 m = bottom of riser).

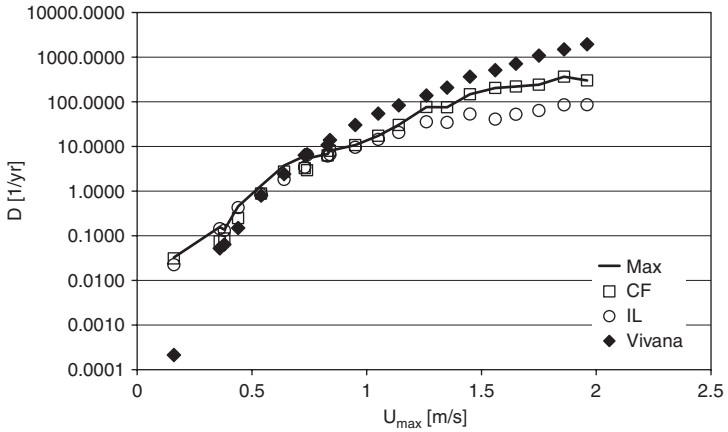

Fig. 18. Fatigue damage as function of maximum current velocity (Max: maximum measured fatigue damage along the riser; CF: maximum measured CF fatigue damage; IL: maximum measured IL fatigue damage; VIVANA: maximum fatigue damage calculated using the theoretical VIV model).

overpredicted by a factor of 8. The high fatigue damage found from the theoretical VIV model is consistent to the overprediction of the response frequency seen from Fig. 13.

8. Conclusions and recommendations

The following is observed for the Hanøytangen cases.

(a) It is shown that the fatigue damage for an SN curve with $m = 3$ should be proportional to U^7 (U is the current velocity) and U^4 when natural frequencies for responding modes are dominated by tension and bending stiffness, respectively. The Hanøytangen riser fatigue is in good agreement with this; with damage going as U^7 for the lowest

current velocities and U4 for the highest. This applies for fatigue from both in-line IIL) and cross-flow (CF) vibrations.

(b) Based on the Hanøytangen data, it seems that the transition velocity between the tension-dominated region and the bending-stiffness-dominated region is equal to the current velocity that gives response at a mode with an equal eigenfrequency for a tensioned string and an untensioned beam.

(c) IL VIV has a significant contribution to fatigue on the Hanøytangen riser for the lowest modes. Fatigue due to CF dominates at the highest currents speeds. Accordingly, IL stresses are the main source of VIV fatigue for tension-dominated risers, while CF stresses are the main source to fatigue for bending-stiffness-controlled risers.

(d) Maximum fatigue damage on the circumference of a riser cross section is in general close either the IL or the CF fatigue damage contribution. A balanced contribution may be found between the transition velocities for IL and CF.

Comparing measurements to calculations with the VIVANA program leads to the following set of conclusions.

(i) The theoretical VIV model is able to identify both relevant mode numbers and frequencies for CF response compared to the test data for dominating mode orders up to 20. For cases with higher current velocities, it seems that the theoretical VIV model gives a systematic overprediction of the response frequency.

(ii) The theoretical VIV model will in general overpredict the fatigue damage from CF vibrations by a factor up to 6 for cases with dominant modes up to about 20. Increasing current speed will lead to increasing overprediction.

(iii) The fatigue damage at the lower end of a riser that is excited at the upper part seems to be overpredicted by the theoretical VIV model by a factor of up to 18. A damping model that favours low spatial attenuation of the response along the riser may cause this.

(iv) The theoretical VIV model assumes that the response takes place at a limited number of discrete frequencies. However, measurements show that the response has a more stochastic nature with many participating response frequencies. This difference is important and calls for further work on response models for cases with a high order of responding eigenfrequencies.

Hopefully, these findings will be useful for the understanding of VIV-analysis results as well the planning of future experiments.

Acknowledgments

The present work has been supported by the Norwegian Deepwater Program, the Norwegian Marine Technology Research Institute (MARINTEK) and the Centre of Excellence on Ships and Ocean Structures (CeSOS) at the Norwegian University of Technology and Science (NTNU).

References

Anzai, H., Endo, T., 1979. On-site fatigue damage under complex loading. International Journal of Fatigue 1 (1), 29.

Baarholm, G.S., Larsen, C.M., Lie, H., Mørk, K., Meling, T.S., 2004. Simplified model for evaluation of fatigue from vortex induced vibrations of marine risers. In: Proceedings of the 23rd International Conference on Offshore Mechanics and Arctic Engineering, OMAE2004-51407, Vancouver, Canada.

Chaplin, J.R., Bearman, P.W., Fontaine, E., Herfjord, K., Isherwood, M., Larsen, C.M., Meneghini, J.R., Moe, G., Triantafyllou, M., 2004. Blind predictions of laboratory measurements of vortex induced vibrations of a tensioned riser. In: Proceedings of the International Flow Induced Vibration Conference, Paris, France.

Det Norske Veritas, 1998. Fatigue Assessment of Ship Structures. Classification Note No. 30.7.

Fylling, I.J., Larsen, C.M., Sødahl, N., Ormberg, H., Engseth, A., Passano, E., Holthe, K., 1995. RIFLEX—Theory Manual. SINTEF Report STF70 F9521.

Gopalkrishnan, R., 1993. Vortex-induced forces on oscillating bluff cylinders. Ph.D. Thesis, MIT, Cambridge, MA, USA.

Huse, E., Kleiven, G., Nielsen, F.G., 1998. Large scale model testing of deep sea risers. In: Proceedings of the Offshore Technology Conference, Houston, TX, OTC 8701.

Huse, E., Kleiven, G., Nielsen, F.G., 1999. VIV-induced axial vibrations in deep sea risers. In: Proceedings of the Offshore Technology Conference, Houston, TX, OTC 10932.

ISSC 2003. In: Proceedings of the 15th International Ships and Offshore Structures Congress, San Diego, USA, 2003.

Kaasen, K.E., Lie, H., 2005. Analysis of measurements from large scale VIV model tests of a riser in linearly sheared flow. Journal of Fluids and Structures, to be submitted.

Larsen, C.M., Bech, A., 1986. Stress analysis of marine risers under lock-in condition. In: Proceeding of the Fifth International Offshore Mechanics and Arctic Engineering Symposium, Tokyo, Japan.

Larsen, C.M., 2000. Empirical VIV models. In: Proceedings of Workshop on Vortex-Induced Vibrations of Offshore Structures, São Paulo, Brazil.

Larsen, C.M., Vikestad, K., Yttervik, R., Passano, E., 2000. VIVANA—Theory Manual. MARINTEK Report MTF00-023.

Larsen, C.M., Vikestad, K., Yttervik, R., Passano, E., 2001. Empirical model for analysis of vortex induced vibrations—theoretical background and case studies. In: Proceedings of 20th International Conference on Offshore Mechanics and Arctic Engineering, Rio de Janeiro, Brazil, OMAE2001/OFT-1203.

Lie, H., Kaasen, K.E., 2005. Modal analysis of measures from a large-scale VIV model test of a riser in linearly sheared flow. Journal of Fluid and Structures, Submitted for publication.

Miner, M.A., 1945. Cumulative Damage in Fatigue. Journal of Applied Mechanics 12, 159–164.

Moe, G., Arntsen, Ø.A., Hoen, C., 2001. VIV analysis of risers by complex modes. In: Proceedings of the International Symposium on Offshore and Polar Engineering, IL-38.

NORSOK Standard 1998. Design of Steel Structures—Annex C—Fatigue Strength Analysis.

Triantafyllou, M.S, Triantafyllou, G.S. Tein, D., Ambrose, B.D., 1999. Pragmatic riser VIV analysis. In: Proceedings of the Offshore Technology Conference, OTC 10931, Houston, USA.

Vandiver, J.K., Lee, L. 2003. SHEAR7 V4.3 Program Theoretical Manual.

Vikestad, K., 1998. Multi-frequency response of a cylinder subjected to vortex shedding and support motions. Ph.D. Thesis, Department of Marine Structures, Norwegian University of Science and Technology, Trondheim, Norway.

Venugopal, M., 1996. Damping and response prediction of a flexible cylinder in a current. Ph.D. Thesis, Department of Ocean Engineering, Massachusetts Institute of Technology, Cambridge, MA, USA

Yttervik, R., Passano, E., Krogstad, J., Larsen, C.M., 2003. VIVANA—User's Manual Version 3.2. MARINTEK Report 516419.02.02.